The Application of Machine Perfusion as an Enhanced *ex vivo* Model for Optical Imaging*

Katie Doyle[1], Morenike Magbagbeola[1], Zainab L. Rai[1,2,3], Dale Waterhouse[1], Lukas Lindenroth[1], George Dwyer[1], Amir Gander[2,3], Agostino Stilli[1], Brian R. Davidson[1,2,3], and Danail Stoyanov[1]

***Abstract*— Optical imaging techniques such as spectral imaging show promise for the assessment of tissue health during surgery; however, the validation and translation of such techniques into clinical practise is limited by the lack of representative tissue models. In this paper, we demonstrate the application of an organ perfusion machine as an *ex vivo* tissue model for optical imaging. Three porcine livers are perfused at stepped blood oxygen saturations. Over the duration of each perfusion, spectral data of the tissue are captured via diffuse optical spectroscopy and multispectral imaging. These data are synchronised with blood oxygen saturation measurements recorded by the perfusion machine. Shifts in the optical properties of the tissue are demonstrated over the duration of the each perfusion, as the tissue becomes reperfused and as the oxygen saturation is varied.**

I. INTRODUCTION

The primary form of imaging used during surgery is performed by conventional colour digital cameras [1]. These replicate human vision by detecting in the red, green, and blue regions of the visible light spectrum [2]. Visible and near-infrared light experiences a wide range of complex interactions with tissue (typical wavelength ranges of 400–1000 nm) [3]. As conventional cameras only capture three channels, most of the information obtained from these interactions is lost and, aside from improvements in magnification, such cameras do not provide any additional enhancement to a surgeon's ability to visually assess tissue viability [4]. Using spectral imaging, the reflectance spectrum of tissue may be captured for a number of spectral bands. Depending on the number of wavelength bands imaged, this technique can be termed multispectral imaging (MSI; up to 10 spectral bands imaged) or hyperspectral imaging (HSI; up to 100 spectral bands imaged) [4]. For simplicity, MSI will be used throughout this article. The increased spectral resolution of MSI over conventional colour imaging allows for more information to be obtained from light-tissue interactions. If a particular compound exhibits light absorption in the analysed wavelength region, absorption measurements at multiple discrete wavelength bands can be used to quantify the compound's concentration. There are many compounds present in biological tissue which, when tracked using MSI, can act as biomarkers capable of providing diagnostic information about the condition of the tissue [3], [4]. Examples include monitoring tissue perfusion by tracking levels of oxyhemoglobin (HbO) and deoxyhemoglobin (DHb) [4]–[6], assessment of edema through the measurement of tissue water content [7], [8], cancer detection through direct classification or functional parameter measurement [6], [9], [10] or evaluating cellular metabolism by monitoring the redox state of cytochrome-c-oxidase [11].

Despite showing promise as an optical assessment tool of tissue health during surgery, there are a number of barriers in the translation of MSI into clinical practise. One such barrier is the difficulty involved in clinically validating potentially useful biomarkers, due to a lack of *ex vivo* models. In order for a biomarker to be useful in a clinical setting, it must be connected with underlying biological processes, and the relevant clinical performance characteristics must be defined [3]. *Ex vivo* human tissue models are typically cadaveric or excised tissue, without oxygenated blood supply. The lack of active blood flow fundamentally alters the optical properties of *ex vivo* tissue, directly affecting its comparability to *in vivo* counterparts [3], [4]. Without an oxygenated blood supply, tissue will begin to degrade in the first few hours post-excision, causing changes in tissue optical properties due to osmosis, shrinkage, and ischaemia [4], [12]. Halting degradation through freezing or fixing are not ideal countermeasures, as these methods also introduce changes in tissue optical properties [13]. Hemoglobin (Hb) is a compound within red blood cells which greatly influences tissue reflectance, due to its large molar extinction coefficient. The impact of Hb on tissue optical properties is greatest in the visible region of the electromagnetic spectrum, where Hb most readily absorbs and scatters light. An increase in Hb concentration causes a corresponding increase in absorption and scattering due to the increased likelihood of light coming into contact with Hb molecules. Additionally, the spectral absorbance of Hb changes depending on blood oxygen content, causing a shift in tissue optical properties as soon as oxygenated blood supply is halted [14].

Organ perfusion machines (PMs) are used in clinical practise to preserve *ex vivo* donor organs by maintaining oxygenated blood supply during organ transport and assessment for transplant surgery [15], [16]. Such machines could also

*This research was funded in whole, or in part, by the Wellcome/EPSRC Centre for Interventional and Surgical Sciences (WEISS) [203145/Z/16/Z]; the Engineering and Physical Sciences Research Council (EPSRC) [EP/P027938/1, EP/R004080/1, EP/P012841/1]; the Royal Academy of Engineering Chair in Emerging Technologies Scheme [CiET1819/2/36]. For the purpose of open access, the authors have applied a CC BY public copyright licence to any author accepted manuscript version arising from this submission.

[1]Wellcome/EPSRC Centre for Interventional and Surgical Sciences (WEISS), University College London, London, UK

[2]Centre for Surgical Innovation, Organ Repair and Transplantation (CSIORT), UCL, London, UK

[3]Royal Free Hospital NHS Trust, London, UK

be utilised in a research setting to provide oxygenated blood flow to *ex vivo* tissue, making it a far more representative model of *in vivo* tissue than unperfused *ex vivo* models [3], [4]. Perfusate parameters such as blood oxygen saturation (SpO_2), temperature, pH, and pressure could be monitored and controlled [16], [17], and additives such as dyes or nano particle solutions could be added in exact quantities for the given blood volume. This approach could aid in increasing the longevity of *ex vivo* human tissue samples, allowing more time for research to be performed, thus maximising the usefulness of a limited resource. Additionally, access to *ex vivo* perfused human tissue could reduce reliance on live animal models.

In previous work, we presented the evaluation of an organ PM, designed as platform for conducting research with perfused, *ex vivo* organs [18]. In this work, we demonstrate the application of the PM as a perfused *ex vivo* tissue model for optical imaging. The paper is structured as follows; in section II, the methodology of each perfusion case is outlined, and spectral acquisition modalities are described. The post-processing and and analysis methods for each modality are also detailed. Section III presents the spectral analysis of each perfusion case, alongside perfusate SpO_2 measurements obtained from the PM. The changes in the optical properties of the organ are measured as the organ is perfused, focusing on the impact of hemoglobin, the dominant absorber. These are compared with SpO_2 levels, recorded by the PM. Finally, section IV concludes the paper and identified as areas of future work.

II. METHODS

A. Liver Perfusion

Three porcine livers, along with autologous blood, were obtained from an abattoir and prepared in the same manner outlined in previous work [18]. After transportation, the liver was prepared to be connected to the perfusion system. The portal vein (PV) and hepatic artery (HA), designated for inflow, and the hepatic vein (HV), designated for outflow, were cannulated using 6.35 mm tubing. Disposable perforated plastic sheeting was used to suspend the liver over the organ chamber, which consisted of a supported metal bowl with a drain feeding directly back to the perfusate reservoir. Once suspended over the organ chamber, the multispectral camera was placed in a fixed position over the liver, and the spectroscopy probe was placed against the surface of the liver using a retort stand and clamp.

The reservoir was filled with 3 l of blood which was circulated through the perfusion system during priming. Once the tubing was primed with blood, the inlet and outlet tubes were clamped, connected to the liver tubing, and unclamped. In each case, the liver was perfused with deoxygenated blood for up to 10 minutes, after which, the oxygen supply to the oxygenator was enabled. The supply of oxygen was increased in stepped intervals over the duration of the experiments, up to a maximum supply pressure of approximately 0.2 bar. The total duration of perfusions was between 60 and 90 minutes in each case. Circulating blood was maintained at a temperature of 29 °C, and SpO_2 was measured by an oxygen sensor for the duration of each perfusion. The location of the oxygen sensor within the perfusion machine flow circuit is indicated in figure 1.

B. Spectral Aquisition

The livers were evaluated using two spectral assessment modalities: MSI and diffuse optical spectroscopy (DOS). Similar to MSI, DOS is a technique which can be used to determine tissue optical properties and their wavelength dependence. DOS permits a far higher spectral resolution than spectral imaging; however, it is performed using a contact-based probe, limiting it to a single spatial dimension and making it more invasive than that of MSI. In contrast, MSI is non-contact, and permits the assessment of two spatial dimensions, usually by sacrificing spectral or temporal resolution. The ability to assess tissue in two spatial dimensions makes it more suitable than DOS for use in surgery, as it can be compared to the surgeon's visual assessment. As DOS provides a high spectral resolution, it is still a useful comparator for MSI.

DOS was carried out by securing a fiber optic reflection probe (RP22 Reflection Probe with Round Leg, Thorlabs Inc., Newton, New Jersey 07860, USA), supplied by a tungsten-halogen light source (SLS201L Stabilized Light Source, Thorlabs Inc., Newton, New Jersey 07860, USA), in a fixed location against the surface of the liver. Reflected light was collected by a charge coupled device spectrometer (CCS200 Compact CCD Spectrometer, Thorlabs Inc., Newton, New Jersey 07860, USA). Spectra (500-1000 nm) were recorded continuously, at a rate of 2 spectra per second, for the duration of the experiment. Calibration measurements with the light source on and off were taken with the probe against a white calibration card (Spyder Checkr, Datacolor, Lawrenceville, New Jersey 08648, USA), and against the liver. A consistent integration time was used for all measurements.

MSI was performed using a filter wheel camera (SpectroCam VIS, Largo, Florida 33777, USA) with 8 bandpass filters (470/20, 480/25, 520/20, 540/18, 560/20, 578/10, 615/17, and 645/17 nm, centre wavelength/full width at half maximum), secured to a tripod and positioned at a fixed focal length located over the liver. Due to data storage restraints, multispectral images (16-bit, 1408×1044 pixels) of the liver were captured in intervals rather than being recorded continuously. Each acquisition interval had a duration of approximately 40 seconds, during which 20 images for each of the 8 filters were taken at a fixed exposure. Image acquisition intervals for each perfusion are displayed in figure 3, (d), (e), and (f). Calibration measurements were taken prior to the liver perfusion by imaging a white calibration card, in place of the liver, at the same position and focal distance.

C. DOF Spectral Processing and Analysis

The raw spectroscopy data were processed and analysed using MATLAB R2021a (Mathworks, 01760 Natick, Massachusetts, USA); a summary schematic of the spectral signal

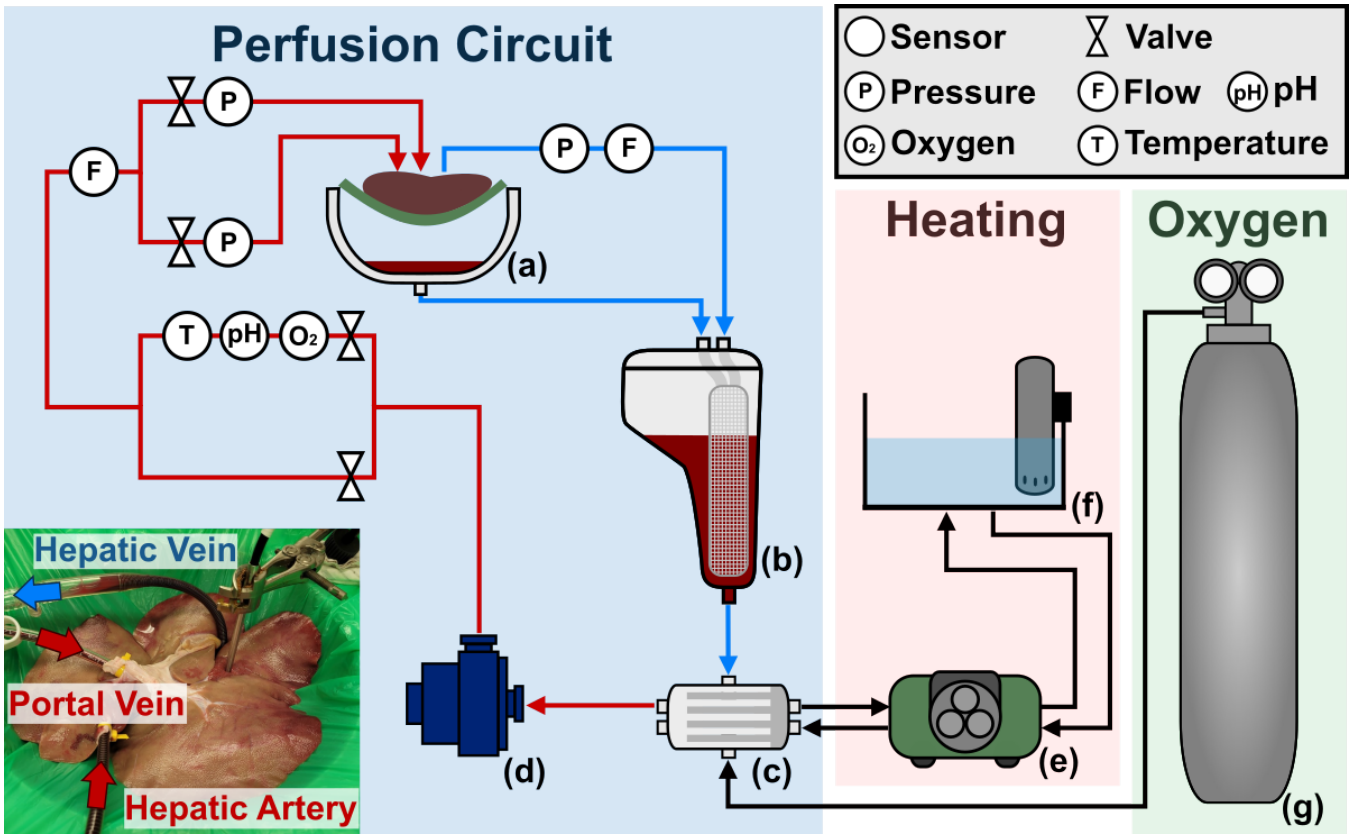

Fig. 1. Schematic of the perfusion system. For further information regarding the system, see [18]. The liver is suspended over the organ chamber, (a), with outflow from the HV leading to the reservoir, (b), where blood is filtered before entering the oxygenator, (c), and recirculated back to the liver by the centrifugal pump, (d). A peristaltic pump, (e), supplies the heat exchanger within the oxygenator with water warmed in the water reservoir, (f). Oxygen gas is supplied to the oxygenator via a canister, (g).

processing workflow is shown in figure 2 (c). The theoretical basis for obtaining the attenuated spectra from the raw acquired spectra is described in section II-C.1.

Following processing, specific landmarks of the HbO and DHb absorption spectra (indicated in figure 2, (b)) were analysed in the attenuated spectra:

- the 760 nm peak height was analysed as a marker of deoxygenated blood, as this peak only exists in the spectrum of DHb
- the ratios of the isosbestic point at 815 nm and the region of greatest difference in spectral intensity at 690 nm of the DHb and HbO spectra.

1) Spectral Processing: The overall tissue absorption coefficient, $\mu_a\ (\lambda)$, depends on the molar concentrations, c_i, of the constituent chromophores, and their molar extinction coefficients, $\varepsilon_i\ (\lambda)$ [14]:

$$\mu_a(\lambda) = \sum_i c_i \cdot \varepsilon_i(\lambda) \tag{1}$$

The Beer-Lambert law can be used to approximate the absorption of diffuse light in tissue during diffuse reflectance spectrometry, where L is the mean light path length through the tissue, $I_0(\lambda)$ is the intensity of light exiting the uniform material, $I(\lambda)$ is the incident intensity of the measured light entering the detector, and $\mu_a(\lambda)$ is the absorption coefficient [14]:

$$I\left(\lambda\right) = I_0\left(\lambda\right) \cdot \exp\left(-\mu_a\left(\lambda\right) \cdot L\right) \tag{2}$$

Equation 2 assumes that there are no scattering contributions to the attenuation of the intensity and that the absorption contributions from the individual absorbing units are independent of each other. Thus, it can only be applied as an approximation if the contribution of absorption is much greater than that of scattering. Rearranging 2 yields:

$$A\left(\lambda\right) = -\ln\left(\frac{I\left(\lambda\right)}{I_0\left(\lambda\right)}\right) = \mu_a\left(\lambda\right) \cdot L \tag{3}$$

Accounting for spectral non-uniformity of the light source, and detector sensitivity, the attenuation, $A(\lambda)$, is defined by the following expression [14], [20]:

$$A\left(\lambda\right) = -ln\left(\frac{I_{raw}\left(\lambda\right) - I_{dark}\left(\lambda\right)}{I_{white}\left(\lambda\right) - I_{dark}\left(\lambda\right)}\right) \tag{4}$$

where I_{raw} is the raw acquired signal, I_{dark} is the reference measurement obtained with the light source off, and I_{white} is the reference measurement obtained with the probe on a white calibration card (uniform diffuse reflectance near unity).

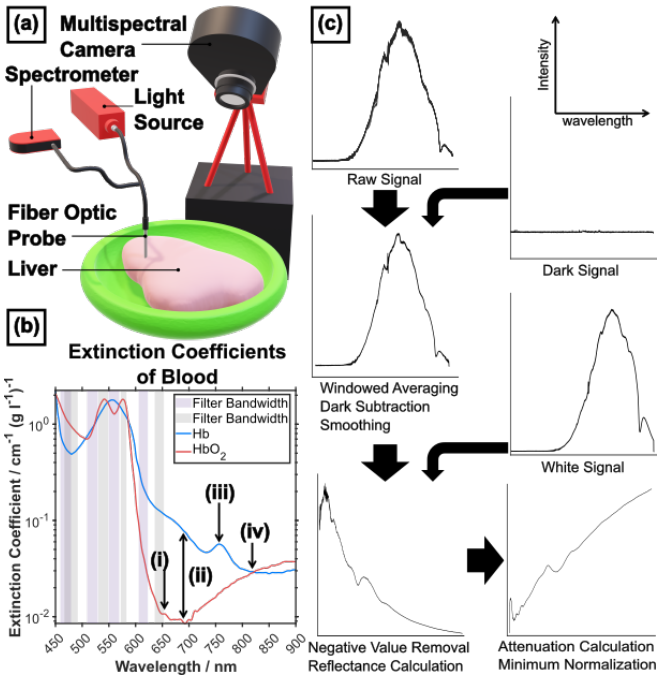

Fig. 2. (a) Diagram of imaging and spectroscopy setup. (b) is the spectra of the extinction coefficients of DHb and HbO, plotted from literature values [19]. Spectral bandwidths imaged by the camera are overlaid in purple and gray. Distinct landmarks in the DHb and HbO spectra, analysed using DOS, are labelled: (b), (i)) is the peak at 660 nm, present in the HbO spectrum only; (b), (ii)) is the region with the greatest difference in spectral intensity at 690 nm; (b), (iii)) is the peak at 760 nm, present in the DHb spectrum only; (d), (iv)) is the isosbestic point at 815 nm. (c) Summary schematic of spectral signal processing workflow.

D. MSI Spectral Processing and Analysis

Processing and analysis of the spectral imaging data was performed using MATLAB; a data cube was assembled for each acquisition by combining the raw image files of each spectral band. To compliment the spectroscopy measurements which compared the isosbestic point between DHb and HbO to the region of greatest difference between DHb and HbO, the ratio of the 645 nm band to the isosbestic at the 520 nm band was compared for the MSI measurements. Additionally, spectral angle mapping (SAM), described in section II-D.1 was used to compare individual MSI datacubes to the overall MSI dataset.

1) Spectral Angle Mapping: Spectral angle mapping (SAM) is used to compare individual multispectral image cubes to the total set of image cubes. An $m \times n$ data matrix is composed from the pixels of all MSI images in the dataset, where m is the number of pixels and $n = 8$ is the number of wavelength bands. Max normalization is performed on each pixel of the data matrix: the intensity value for each wavelength band is divided by the maximum intensity value of all wavelength bands for that pixel. k-means clustering is applied to the data matrix to group pixels with similar spectral characteristics. Pixels are grouped into $k = 3$ clusters, resulting in a 3×8 matrix containing the 3 cluster centroids for each of the 8 wavelength bands (Figure 3, (g)). Each of the cluster centroids are normalized: the 8 columns are divided by the Euclidian normal of each row.

Individual multispectral image cubes are then compared pixel-by-pixel to the cluster centroid matrix using SAM. The SAM algorithm is run upon each pixel in an MSI image, where the reference dataset, r, is an 8×1 matrix representing the MSI pixel and the target dataset, t, is the 3×8 matrix of cluster centroids. This results in a 3×1 matrix to represent each pixel. The spectral angle is the angle between two spectra in n-dimensional space, where n is the number of wavelength bands. It is computed using the dot product of the two spectra, divided by the product of their magnitudes. The result is a measure of how similar the two spectra are, with angles closer to 0° indicating greater similarity [21]. The equation for calculating the spectral angle is defined as [21], [22]:

$$\theta = cos^{-1}\left(\frac{\vec{t} \cdot \vec{r}}{|| \vec{t} || \cdot || \vec{r} ||}\right) \quad (5)$$

III. RESULTS AND DISCUSSION

An analysis of the peak heights of absorption spectra recorded via DOS are shown in Figure 3 (a), (b), and (c). In each case, as the relative change in the spectral properties of the tissue was being examined across time, the probe was to remain at a fixed position. As the spectroscopy probe only has 1-D spatial resolution, measurements recorded were extremely sensitive to any changes in position. As a result, the DOS measurements analysed do not span the entirety of the perfusion, as only measurements when the probe was securely fixed in position could be included. With the exception of liver 3, measurements taken before the perfusion commenced are included for both the MSI and DOS datasets, highlighting the difference in optical properties between perfused and unperfused tissue.

A. Liver 1

Between 25 and 38 minutes, the 760 nm peak increases, while the 660 nm peak decreases, indicating an increasing ratio of DHb to HbO. This reflects the SpO_2 measurements; the majority of the Hb entering the liver during this time is still predominantly DHb. In the same timeframe, there is an increase in the 690 nm peak and a more marginal increase in the 815 nm peak. As 815 nm is the isosbestic point, any change in this peak will denote a fluctuation in the total Hb. Between 38 and 43 minutes, the 760 nm peak decreases in height and the 660 nm peak increases, showing an increase in oxygenation, after a lowpoint at 38 minutes. Oxygenation then decreases between 43 and 49 minutes. While the SpO_2 of blood entering the liver was increasing, the decrease in oxygenation seen in the spectroscopy results could be due to an uptick in cellular metabolism.

In the imaging results (Figure 3, (d)), the isosbestic point in the 520 nm band follows a similar pattern to the 815 nm isosbestic point in the spectroscopy results. The highest point in the absorption in the 520 nm band is at 39 minutes, coinciding with the increase in the 815 nm peak. Throughout the perfusion, the absorption of the 615 nm band increases, reaching a maximum around 39 minutes, before decreasing

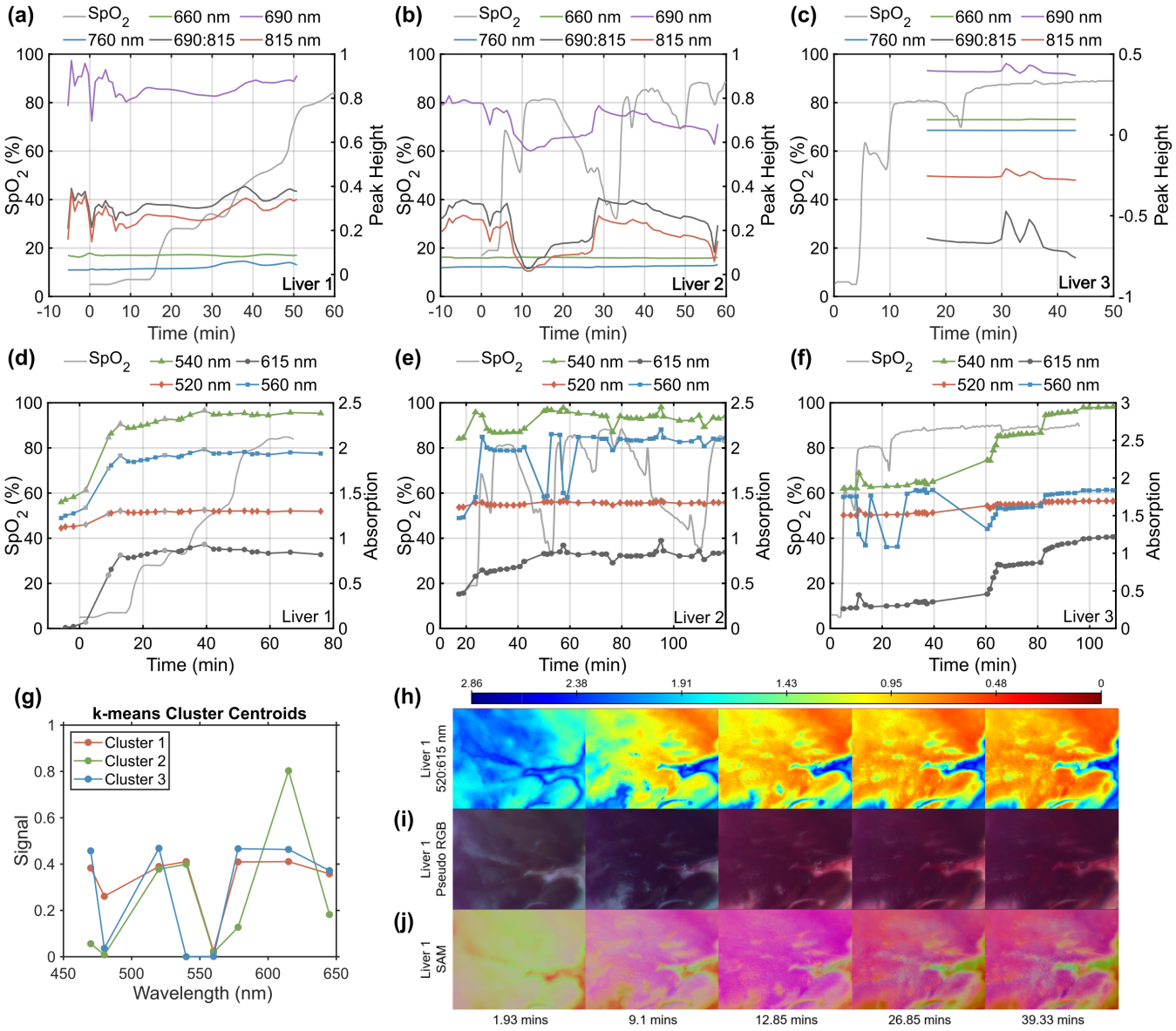

Fig. 3. Top: comparison of SpO_2, measured by the perfusion system oxygen sensor, and peak heights of attenuated spectra measured by the spectrometer for liver 1 (a), liver 2 (b), and liver 3 (c). Middle: comparison of SpO_2, measured by the perfusion system oxygen sensor, and the average absorption for the 520, 540, 560, and 615 nm bands imaged by the multispectral camera for liver 1 (d), liver 2 (e), and liver 3 (f). (g) is the cluster centroids generated by k-means clustering for each wavelength band used in the creation of the spectral angle mapping (SAM) images in (j). (h) is a colormapped representation of the ratio of the 520 (isosbestic) and 615 nm bands. (i) is a pseudo RGB image set generated from the 645, 540 and 470 nm bands. (j) is a SAM comparison of the cluster centroids in (g) and individual images, where the comparisons with clusters 1, 2, and 3 are mapped to the red, green, and blue channels, respectively. Additional gray markers in (d) indicate the timestamps of the multispectral images for liver 1 displayed in (h), (i), and (j).

for the rest of the duration of the perfusion. Again, the peak at 39 minutes corresponds well to the peak height changes of the spectrometer measurements, showing that this was not a localised change. Colormapped images are included for Liver 1, shown in Figure 3, (h), (i), and (j). The shift in tissue optical properties is most pronounced when the tissue moves from an unperfused to a perfused state. Figure 3, (j) compares individual images to 3 clusters generated from the overall dataset. The earliest image at 1.93 minutes is largely yellow and green, indicating that a mixture of clusters 1 and 2 are most representative of this image. In the two images after, at 9.1 and 12.85 minutes, magenta becomes the dominant color, indication a mixture of clusters 1 and 3. In the final two images, 26.85 and 39.33 minutes, the dominant color is still magenta, but with more red, indicating an increased leaning towards cluster 1.

B. Liver 2

At 18 minutes, the level of blood in the reservoir began to become depleted, while consistent outflow from the liver was not yet established. 80 ml of saline was added to the reservoir which resulted in a decrease in the measured SpO_2 from the sensor. Oxygen supply was decreased as a precaution;

however, at 33 minutes, the oxygenator caused the perfusate to develop bubbles which disrupted the oxygen sensor. The oxygen supply was further reduced until the issue with the oxygenator was resolved. It is likely, therefore, that the SpO_2 readings are unreliable and the true SpO_2 was lower than the values measured by the sensor. Over the duration of the perfusion, the 760 nm peak gradually increased while the 660 nm peak decreased, indicating a steady increase in DHb and a corresponding decrease in HbO. Comparing the isosbestic points, fluctuations in the total Hb can be seen in both the spectroscopy data and imaging data at numerous timestamps, such as the maxima at 6, 28, and 37 minutes, and the minima at 10 and 57 minutes.

C. Liver 3

In the time intervals recorded, all peak heights remain quite stable, consistent with the SpO_2 data. There are two increases in the 690 and 815 nm peak heights at 31 and 35 minutes, which are also present in the 520 and 615 nm bands, indicating a global fluctuation in total Hb during this period. Over the duration of this perfusion, there is a gradual increase in the 660 nm peak and decrease in the 760 nm peak, while the peak height of the isosbestic point marginally decreases. This implies a gradual increase in HbO, alongside a decrease in total Hb. Contrary to the spectroscopy data, the isosbestic point at the 520 nm band in the MSI data indicates an increase in total Hb over the duration of the perfusion. This indicates that the decrease in total Hb was localised to the area monitored by DOS probe, and not to the liver as a whole. The absorption of the other bands are also seen to increase during the remainder of the perfusion and even after perfusion has stopped. This may be indicative of tissue degradation and warrants further investigation. No compounds were added to the perfusate to maintain metabolic activity, osmotic balance, or oncotic balance, and therefore gradual degradation of the tissue is to be expected. In order to adequately assess the effectiveness of the PM at maintaining tissue optical properties, longer perfusion times, and a control will be included in future work.

IV. CONCLUSION

The perfusion system facilitated the measurement of the shift in the optical properties of the tissue as it was perfused. As expected, the total tissue Hb and the SpO_2 both had a notable influence on the optical properties of the tissue. The data discussed in this paper were recorded during a preliminary assessment phase of the PM, alongside the measurement of other performance criteria specific to the PM itself. As such, the methodology of these experiments was performed in a demonstrative capacity within certain constraints. Improvements to both the PM system and methodology have been identified. The former would increase the effectiveness of the PM as a testbed for optical imaging modalities; the latter would permit a more quantitative assessment of future optical data collected. Improvements to the PM include:

- the addition of an oxygen sensor on the outflow from the organ would enable the quantification of the total reduction in SpO_2 between the blood entering and exiting the organ; these could be compared to tissue SpO_2 estimation determined by spectral analysis;
- the addition of load cells onto the mount for the organ chamber in order to record the change in weight of the organ as it is perfused; this could be compared with spectral assessments of total Hb;
- automated control of the oxygen supply valve, to allow for more precise and repeatable changes in oxygen supplied to the blood.

Improvements to the methodology include:

- inclusion of a control in the form of a liver containing some blood but which is not undergoing any form of perfusion;
- a repeat of the procedure of the original experiments with changes in the stepping of the oxygen supply, such as a reversal (commencing at the highest oxygen supply), or cyclic stepping of oxygen supply (stepping oxygen supply up, then down, in a cyclic fashion);
- increased data storage and automation of image capture to gather imaging data with an improved temporal resolution.

REFERENCES

[1] Daniel J. Mirota, Masaru Ishii, and Gregory D. Hager. Vision-based navigation in image-guided interventions. *Annual Review of Biomedical Engineering*, 13:297–319, 2011.

[2] Yasushi Imamoto and Yoshinori Shichida. Cone visual pigments. *Biochimica et Biophysica Acta - Bioenergetics*, 1837(5):664–673, 2014.

[3] Dale J. Waterhouse, Catherine R.M. Fitzpatrick, Brian W. Pogue, James P.B. O'Connor, and Sarah E. Bohndiek. A roadmap for the clinical implementation of optical-imaging biomarkers. *Nature Biomedical Engineering*, 3(5):339–353, 2019.

[4] Neil T. Clancy, Geoffrey Jones, Lena Maier-Hein, Daniel S. Elson, and Danail Stoyanov. Surgical spectral imaging. *Medical Image Analysis*, 63:101699, jul 2020.

[5] Neil T Clancy, Shobhit Arya, Danail Stoyanov, Mohan Singh, George B Hanna, and Daniel S Elson. Intraoperative measurement of bowel oxygen saturation using a multispectral imaging laparoscope. *Biomedical optics express*, 6(10):4179–4190, 2015.

[6] Guolan Lu and Baowei Fei. Medical hyperspectral imaging: a review. *Journal of biomedical optics*, 19(1):010901–010901, 2014.

[7] Amadeus Holmer, Jörg Marotz, Philip Wahl, Michael Dau, and Peer W. Kämmerer. Hyperspectral imaging in perfusion and wound diagnostics – methods and algorithms for the determination of tissue parameters. *Biomedical Engineering / Biomedizinische Technik*, 63(5):547–556, oct 2018.

[8] M. Dietrich, S. Marx, M. von der Forst, T. Bruckner, F.C.F. Schmitt, M.O. Fiedler, F. Nickel, A. Studier-Fischer, B.P. Müller-Stich, T. Hackert, T. Brenner, M.A. Weigand, F. Uhle, and K. Schmidt. Bedside hyperspectral imaging indicates a microcirculatory sepsis pattern - an observational study. *Microvascular Research*, 136(December 2020):104164, jul 2021.

[9] Zhimin Han, Aoyu Zhang, Xiguang Wang, Zongxiao Sun, May D Wang, and Tianyu Xie. In vivo use of hyperspectral imaging to develop a noncontact endoscopic diagnosis support system for malignant colorectal tumors. *Journal of biomedical optics*, 21(1):016001–016001, 2016.

[10] Sergio E Martinez-Herrera, Yannick Benezeth, Matthieu Boffety, Jean-François Emile, Franck Marzani, Dominique Lamarque, and François Goudail. Multispectral endoscopy to identify precancerous lesions in gastric mucosa. In *Image and Signal Processing: 6th International Conference, ICISP 2014, Cherbourg, France, June 30–July 2, 2014. Proceedings 6*, pages 43–51. Springer, 2014.

[11] Luca Giannoni, Frédéric Lange, Marija Sajic, Kenneth J. Smith, and Ilias Tachtsidis. hNIR: a hyperspectral imaging system for mapping changes in haemoglobin and cytochrome-c-oxidase on the exposed cerebral cortex of mice. In *Biophotonics Congress 2021*, volume 27, page BW3B.5, Washington, D.C., 2021. OSA.

[12] Pei-Lin Hsiung, Prashant R. Nambiar, and James G. Fujimoto. Effect of tissue preservation on imaging using ultrahigh resolution optical coherence tomography. *Journal of Biomedical Optics*, 10(6):064033, 2005.

[13] Martin G. Shim and Brian C. Wilson. The effects of ex vivo handling procedures on the near-infrared Raman spectra of normal mammalian tissues. *Photochemistry and Photobiology*, 63(5):662–671, 1996.

[14] Irving J. Bigio and Sergio Fantini. *Quantitative Biomedical Optics: Theory, Methods, and Applications*. Cambridge Texts in Biomedical Engineering. Cambridge University Press, jan 2016.

[15] Hynek Mergental, Richard W. Laing, Amanda J. Kirkham, M. Thamara P.R. Perera, Yuri L. Boteon, Joseph Attard, Darren Barton, Stuart Curbishley, Manpreet Wilkhu, Desley A.H. Neil, Stefan G. Hübscher, Paolo Muiesan, John R. Isaac, Keith J. Roberts, Manuel Abradelo, Andrea Schlegel, James Ferguson, Hentie Cilliers, Julian Bion, David H. Adams, Chris Morris, Peter J. Friend, Christina Yap, Simon C. Afford, and Darius F. Mirza. Transplantation of discarded livers following viability testing with normothermic machine perfusion. *Nature Communications*, 11(1), 2020.

[16] David Nasralla, Constantin C. Coussios, Hynek Mergental, M. Zeeshan Akhtar, Andrew J. Butler, Carlo D.L. Ceresa, Virginia Chiocchia, Susan J. Dutton, Juan Carlos García-Valdecasas, Nigel Heaton, Charles Imber, Wayel Jassem, Ina Jochmans, John Karani, Simon R. Knight, Peri Kocabayoglu, Massimo Malagò, Darius Mirza, Peter J. Morris, Arvind Pallan, Andreas Paul, Mihai Pavel, M. Thamara P.R. Perera, Jacques Pirenne, Reena Ravikumar, Leslie Russell, Sara Upponi, Chris J.E. Watson, Annemarie Weissenbacher, Rutger J. Ploeg, and Peter J. Friend. A randomized trial of normothermic preservation in liver transplantation. *Nature*, 557(7703):50–56, 2018.

[17] Dilmurodjon Eshmuminov, Dustin Becker, Lucia Bautista Borrego, Max Hefti, Martin J. Schuler, Catherine Hagedorn, Xavier Muller, Matteo Mueller, Christopher Onder, Rolf Graf, Achim Weber, Philipp Dutkowski, Philipp Rudolf von Rohr, and Pierre Alain Clavien. An integrated perfusion machine preserves injured human livers for 1 week. *Nature Biotechnology*, 38(2):189–198, 2020.

[18] M. Magbagbeola, K. Doyle, Z.L. Rai, L. Lindenroth, G. Dwyer, A. Stilli, B.R. Davidson, and D. Stoyanov. Evaluation of A Novel Organ Perfusion Research Platform. In *2022 44th Annual International Conference of the IEEE Engineering in Medicine I& Biology Society (EMBC)*, volume 2022, pages 2565–2568. IEEE, jul 2022.

[19] Nienke Bosschaart, Gerda J. Edelman, Maurice C. G. Aalders, Ton G. van Leeuwen, and Dirk J. Faber. A literature review and novel theoretical approach on the optical properties of whole blood. *Lasers in Medical Science*, 29(2):453–479, mar 2014.

[20] Alexander A. Stratonnikov and Victor B. Loschenov. Evaluation of blood oxygen saturation in vivo from diffuse reflectance spectra. *Journal of Biomedical Optics*, 6(4):457, 2001.

[21] F.A. Kruse, A.B. Lefkoff, J.W. Boardman, K.B. Heidebrecht, A.T. Shapiro, P.J. Barloon, and A.F.H. Goetz. The spectral image processing system (SIPS)—interactive visualization and analysis of imaging spectrometer data. *Remote Sensing of Environment*, 44(2-3):145–163, may 1993.

[22] Jonghee Yoon, James Joseph, Dale J. Waterhouse, A. Siri Luthman, George S. D. Gordon, Massimiliano di Pietro, Wladyslaw Januszewicz, Rebecca C. Fitzgerald, and Sarah E. Bohndiek. A clinically translatable hyperspectral endoscopy (HySE) system for imaging the gastrointestinal tract. *Nature Communications*, 10(1):1902, dec 2019.